

Leveraging Pre-trained Models for FF-to-FFPE Histopathological Image Translation

Qilai Zhang

Shenzhen International Graduate School
Tsinghua University
Shenzhen, China
zhang-ql22@mails.tsinghua.edu.cn

Jiawen Li

Shenzhen International Graduate School
Tsinghua University
Shenzhen, China
lijiawen21@mails.tsinghua.edu.cn

Peiran Liao

Shenzhen International Graduate School Medical Optical Technology R&D Center
Tsinghua University
Shenzhen, China
lpr22@mails.tsinghua.edu.cn

Jiali Hu

Research Institute of Tsinghua
Guangzhou, China
maggie_0225@126.com

Tian Guan

Shenzhen International Graduate School
Tsinghua University
Shenzhen, China
guantian@sz.tsinghua.edu.cn

Anjia Han*

Department of Pathology
The First Affiliated Hospital of Sun Yat-sen University
Guangzhou, China
hananjia@mail.sysu.edu.cn

Yonghong He*

Shenzhen International Graduate School
Tsinghua University
Shenzhen, China
heyh@sz.tsinghua.edu.cn

Abstract—The two primary types of Hematoxylin and Eosin (H&E) slides in histopathology are Formalin-Fixed Paraffin-Embedded (FFPE) and Fresh Frozen (FF). FFPE slides offer high quality histopathological images but require a labor-intensive acquisition process. In contrast, FF slides can be prepared quickly, but the image quality is relatively poor. Our task is to translate FF images into FFPE style, thereby improving the image quality for diagnostic purposes. In this paper, we propose Diffusion-FFPE, a method for FF-to-FFPE histopathological image translation using a pre-trained diffusion model. Specifically, we employ a one-step diffusion model as the generator and fine-tune it with LoRA adapters using adversarial learning objectives. To ensure that the model effectively captures both global structural information and local details, we propose a multi-scale feature fusion (MFF) module. This module utilizes two VAE encoders to extract features of varying image sizes and performs feature fusion before feeding them into the UNet. Furthermore, we utilize a pre-trained vision-language model for histopathology as the backbone for the discriminator to further improve performance. We conducted FF-to-FFPE translation experiments on the TCGA-NSCLC datasets, and our method achieved better performance compared to other methods. The code and models are released at <https://github.com/QilaiZhang/Diffusion-FFPE>.

Index Terms—Image Translation, Histopathology, Diffusion Models

I. INTRODUCTION

Hematoxylin and Eosin (H&E) slides in histopathology are categorized into two primary types based on their prepara-

tion methods: Formalin-Fixed Paraffin-Embedded (FFPE) and Fresh Frozen (FF). FFPE, the more commonly used method in pathological examinations, involves a complex preparation process typically spanning 24 to 48 hours [1]. While FFPE preserves glandular and cellular structure well, the lengthy preparation time makes it unsuitable for rapid pathological diagnosis during surgery. In contrast, FF slides are prepared by freezing tissues in a low-temperature environment, a process that takes only about 15 minutes. FF slides are preferred for rapid diagnosis during surgery to facilitate prompt development of treatment plans [2]. However, when frozen sections are prepared, the tissue tends to become fragile and brittle. In addition, water in the tissue can easily form ice crystals, leading to visual artefacts that can subsequently affect the pathologist’s diagnosis. [3]. With the development of deep learning, in particular generative networks, it has become possible to achieve style transformation between image domains. By applying this style transfer technology to the field of computational pathology, the translation of frozen sections to paraffin sections can improve the readability of digital pathology images. This advance has significant potential for intra-operative pathology diagnosis. [4].

The goal of FF-to-FFPE histopathological image translation is to convert FF images into the style of FFPE images while preserving their original content. Due to the difficulty of obtaining pixel-level matched data pairs of FF and FFPE sections, unpaired image translation methods are required. Generative Adversarial Networks (GANs) [5] such as CycleGAN [6] and CUT [7] are utilized in this context, employing

*Corresponding author. The work is supported by Shenzhen Engineering Research Centre (No. XMHT20230115004), Science and Technology Research Program of Shenzhen City (No. KCXFZ20201221173207022), and Jilin Fuyuan Guan Food Group Co., Ltd. In.

adversarial learning objectives to optimize networks. This ensures content preservation either through cycle consistency or contrastive learning mechanisms. The existing methods [8]–[10] mainly uses GANs to perform FF to FFPE image translation, focusing mainly on improving the preservation of histopathological structures and increasing the inference efficiency. However, these methods typically require training from scratch, requiring a significant amount of data to achieve satisfactory generalization performance [8].

In recent years, generative models such as Stable Diffusion have demonstrated remarkable capabilities in natural image generation [11]–[13]. These pre-trained models effectively capture common image features, making them highly versatile. When fine-tuned for the pathology image domain, the prior knowledge embedded in pre-trained models helps to capture the texture and structure of histopathology images [14], thereby improving the generative performance and generalization ability. Moreover, the advent of pre-trained histopathology vision models has significantly improved the performance of downstream tasks [15]–[17]. Using these pre-trained histopathology models as the backbone of the discriminator can be beneficial for training GANs [18].

Based on the above concepts, we propose a method for FF-to-FFPE histopathological image translation by leveraging pre-trained models, called Diffusion-FFPE. We maintain the adversarial learning objective of GANs by using a pre-trained generative model as the generator and a pre-trained visual model as the discriminator, thus fully exploiting the prior knowledge embedded in the pre-trained models. Inspired by *img2img-turbo* [19], we employ a one-step diffusion model as the generator, fine-tuning it with LoRA adapters [20] using adversarial learning objectives. Specifically, the latent diffusion model [12] includes a VAE encoder, a VAE decoder, a UNet, and a text encoder. We keep the original weights of VAE and UNet fixed and add trainable LoRA adapters to them. In addition, we use CONCH [15], a pre-trained visual model specialized for histopathology, as the backbone of the discriminator to further improve performance.

Since histopathological images contain both global structural information, such as tissue contours, and local details, such as nuclei, we further propose a multi-scale feature fusion (MFF) module to ensure that the model effectively captures both types of information. We use a local VAE encoder and a global VAE encoder to extract features at different image scales and perform feature fusion before feeding them into the UNet. To capture the fine-grained details of histopathological images, we maintain the skip connections between the VAE encoder and the VAE decoder, passing the fused features from the encoder to the decoder.

In summary, the main contributions of this paper are as follows:

- This paper proposes Diffusion-FFPE, a method that leverages pre-trained models for both the generator and discriminator in the task of FF-to-FFPE histopathological translation.

- This paper proposes a multi-scale feature fusion (MFF) module to capture information from histopathological images at various scales, which helps to generate finer details.
- The method achieves state-of-the-art generation performance on the TCGA-NSCLC datasets, outperforming other open-source methods.

II. RELATED WORK

A. FF-to-FFPE Image Translation

Existing methods mainly utilize the GAN-based network for FF-to-FFPE image translation. AI-FFPE [8] introduced a spatial attention module into the generator, which focuses on artifact regions in FF images. This approach also incorporated a self-regularization term between input FF images and generated FFPE images to prevent the creation of clinically misleading data. FastFF2FFPE [9] proposed a GAN-based method that reduces computational costs and accelerates processing times. This method decomposes FF images into low-frequency and high-frequency components using a Laplacian Pyramid and introduces a contrastive learning loss term to enhance the similarity between the original and generated images. ST-MKSC [10] developed a CUT-based network with a multi-frequency domain hierarchical constraint to effectively capture information at different frequencies, thereby minimizing the loss of nuclear detail and improving the removal of artifacts. Additionally, this method proposed the released constraint loss to weaken the constraints of the L1 loss.

Unlike the aforementioned methods, the approach presented in this paper does not involve training a GAN from scratch. Instead, it fine-tunes a pre-trained generative model to improve its generative performance.

B. Unpaired Image Translation with Diffusion Models

In recent years, several methods utilizing diffusion models for unpaired image translation have emerged. EGSDE [21] proposed a image translation method based on diffusion models. In this method, an unconditional diffusion model is trained on the target domain and additional classifiers are trained to distinguish images from different domains. These classifiers are then used to guide the image generation process in the target domain.

On the other hand, DDIBs [22] and CycleDiffusion [23] achieve mapping between image domains by leveraging the latent space of deterministic diffusion models. They transform images into the latent space using the diffusion model of the original domain and then generate images using the diffusion model of the target domain based on this latent representation.

However, these methods require multi-step sampling, resulting in slower inference speeds that do not meet the requirements of fast translation for diagnosis. In addition, they perform poorly in preserving image structure [19], making them unsuitable for pathology image translation.

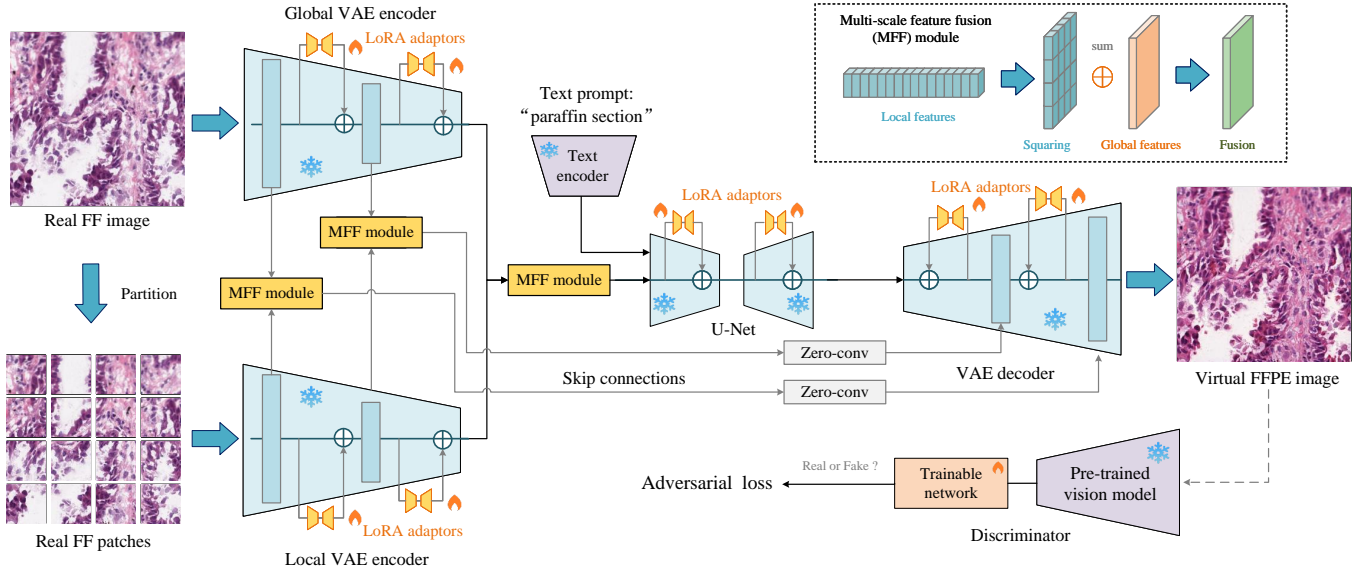


Fig. 1. Overview of Diffusion-FFPE. In the generator, the global VAE encoder extracts features from the entire FF image, and the local VAE encoder extracts features from smaller patches. The features of each layer in the global and local VAE encoders are fused by the multiscale feature fusion (MFF) module. During training, the weights of the VAE and UNet are fixed and trainable LoRA adapters are added. The discriminator uses a pre-trained vision model as its backbone, followed by a trainable classifier.

III. METHODS

The overall structure of Diffusion-FFPE is illustrated in Fig. 1. The network primarily consists of the generator G and the discriminator D . To leverage prior knowledge from pre-trained models, we employ a pre-trained one-step diffusion model with trainable LoRA adapters as the generator, while utilizing a pre-trained vision model as the discriminator’s backbone. During the training phase, we fine-tune the diffusion model with LoRA adapters using adversarial optimization objectives, and employ the multi-scale feature fusion module to improve the model’s focus on local image details. In the inference phase, we utilize the fine-tuned generator to translate FF images into the FFPE image domain.

A. The Generator with a Pre-trained Diffusion Model

Inspired by img2img-turbo [19], we adopt the one-step diffusion model SD-turbo as the generator G , which consists of a VAE encoder \mathcal{E} , a VAE decoder \mathcal{D} , a UNet ϵ_θ , and a text encoder τ_θ . First, the VAE encoder \mathcal{E} extracts features from the image x and converts them into the latent space to obtain the latent representation $z_x = \mathcal{E}(x)$. The text encoder τ_θ converts the text prompt c_Y into the text representation $\tau_\theta(c_Y)$. Both the image latent representation z_x and the text representation $\tau_\theta(c_Y)$ are then fed into the UNet to predict the noise $\epsilon = \epsilon_\theta(z_x, t, \tau_\theta(c_Y))$. Using the predefined schedule s , the predicted noise is utilized to compute the denoised latent representation $z_y = s.step(z_x, \epsilon, t)$. Finally, the VAE decoder \mathcal{D} decodes the image latent representation z_y to obtain the translated image $y = \mathcal{D}(z_y)$.

To enable the pre-trained model to learn the data distribution of histopathological images, we add trainable LoRA adapters to each layer of the VAE and UNet. Additionally, we add skip

connections between the VAE encoder and the VAE decoder to preserve image details and prevent information loss during encoding. We input the features F_x^i extracted from layer i of the VAE encoder \mathcal{E} into the corresponding layers of the VAE decoder \mathcal{D} :

$$F_y^i = \mathcal{D}_i(F_y^{i-1}) + z_\theta(F_x^i), \quad (1)$$

where z_θ denotes zero convolutions layer with weights initialized to zeros.

B. Multi-Scale Feature Fusion

To allow the model to focus on smaller regions, we design a multi-scale feature fusion (MFF) module. First, we divide the image x_{global} into several small patches $\{x_m\}_{m=1}^M$. We then employ a global VAE encoder $\mathcal{E}_{\text{global}}$ to extract global feature F_{global} from the entire image and a local VAE encoder $\mathcal{E}_{\text{local}}$ to extract local features $\{F_m\}_{m=1}^M$ from small patches. Notably, $\mathcal{E}_{\text{global}}$ and $\mathcal{E}_{\text{local}}$ denote the encoder part of the VAE, which obtains the features before transforming them into a distribution and sampling latents from the distribution:

$$F_{\text{global}} = \mathcal{E}_{\text{global}}(x_{\text{global}}), \quad (2)$$

$$F_m = \mathcal{E}_{\text{local}}(x_m). \quad (3)$$

For each layer i of both the global VAE encoder and the local VAE encoder, we concatenate several local features to match the global feature based on their original positional information, and then sum them to obtain the fused features F_{fused} :

$$F_{\text{fused}}^i = F_{\text{global}}^i + \text{concat}(\{F_m^i\}_{m=1}^M). \quad (4)$$

Subsequently, the fused features from the intermediate layers are forwarded to the VAE decoder \mathcal{D} via skip connections

as illustrated in (1). The fused feature F_{fused}^N from the last layers N is transformed into a distribution and a latent variable z_x is sampled from this distribution:

$$z_x = \mathcal{E}_{last}(F_{fused}^N), \quad (5)$$

where \mathcal{E}_{last} denotes the last layer of the VAE encoder.

C. The Discriminator with a Pre-trained Vision Model

To increase the training efficiency, we use a pre-trained visual model Θ for histopathology as the backbone of the discriminator D . We adopt the vision-aided GAN approach [18], where the weights of the pre-trained visual model are kept fixed, followed by a small classifier head C :

$$D(x) = C(\Theta(x)). \quad (6)$$

D. Adversarial Learning Objective

Diffusion-FFPE is trained based on the formulation of CycleGAN [6], which consists of two mapping functions: $G_Y(x, c_Y) : X \rightarrow Y$ and $G_X(y, c_X) : Y \rightarrow X$. The G_X and G_Y networks have the same structure as described in Section III-A. They share UNet weights but have different VAE encoders and VAE decoders. Additionally, they receive different texts c_X and c_Y to perform their respective translation tasks.

To apply adversarial losses to the mapping functions G_X and G_Y , we employ discriminators D_X and D_Y respectively, as described in Section III-C. This ensures that the generated output images match the target domain. The adversarial objective L_{adv} is defined as:

$$\begin{aligned} L_{adv} = & E_y[\log D_Y(y)] \\ & + E_x[\log(1 - D_Y(G_Y(x, c_Y)))] \\ & + E_x[\log D_X(x)] \\ & + E_y[\log(1 - D_X(G_X(y, c_X)))]]. \end{aligned} \quad (7)$$

The cycle consistency loss ensures that when an FF image x is mapped through G_Y to generate an FFPE image $G_Y(x, c_Y)$ and then mapped back through G_X , it should return to the original image x . This can be expressed as $G_X(G_Y(x, c_Y), c_X) \approx x$. Besides, the reconstruction loss L_{rec} is used to measure the similarity between the images.

$$\begin{aligned} L_{cyc} = & E_x[L_{rec}(G_X(G_Y(x, c_Y), c_X), x)] \\ & + E_y[L_{rec}(G_Y(G_X(y, c_X), c_Y), y)], \end{aligned} \quad (8)$$

$$L_{rec} = \lambda_1 L_1 + \lambda_p L_p. \quad (9)$$

The reconstruction loss is formed by a linear combination of the L_1 norm and the Learned Perceptual Image Patch Similarity [24] (LPIPS) L_p , where λ_1 and λ_p are parameters of the linear combination. Additionally, an identity regularization loss L_{idt} is applied to ensure that the generator does not alter images from the target domain.

$$\begin{aligned} L_{idt} = & E_x[L_{rec}(G_X(x, c_X), x)] \\ & + E_y[L_{rec}(G_Y(y, c_Y), y)]. \end{aligned} \quad (10)$$

In general, the overall optimization objective is represented as follows:

$$L_{total} = \lambda_{adv} L_{adv} + \lambda_{cyc} L_{cyc} + \lambda_{idt} L_{idt}. \quad (11)$$

Here, the total loss L_{total} is weighted by the hyperparameters λ_{adv} , λ_{cyc} and λ_{idt} .

IV. EXPERIMENTS

A. Datasets

We perform FF-to-FFPE translation experiments on the TCGA non-small cell lung cancer (TCGA-NSCLC) dataset. For training, we extract 1,367 FF WSIs and 714 FFPE WSIs. For testing, we use 206 FF WSIs and 383 FFPE WSIs, corresponding to the same slides used in AI-FFPE [8]. The WSIs are then cropped into multiple 512x512 patches at 20x magnification. We use a subset of 50,000 pairs of FF and FFPE patches for training due to the large number of patches obtained. We use 2000 FFPE images as the validation dataset for evaluation during training and 10000 FFPE images as the test dataset for final evaluation.

B. Implementation Details

For the pre-trained model, we utilize the one-step diffusion model, SD-turbo [25], as the generator and a pre-trained vision model for histopathology, CONCH [15], as the discriminator. We fixed the weights of the pre-trained model during training. The network is implemented using PyTorch and trained on an NVIDIA A100 Tensor Core GPU for 50,000 training steps with a batch size of 1.

For optimization, we employ the Adam optimizer [26] with an initial learning rate of 5×10^{-6} , and momentum parameters β_1 is 0.9 and β_2 is 0.999. For the loss function L_{rec} , the linear combination parameter λ_1 is set to 1 for both L_{idt} and L_{cyc} . Within L_{cyc} , λ_p is 10, whereas within L_{idt} , λ_p is 1. The weights assigned to the total loss L_{total} are $\lambda_{adv} = 0.5$, $\lambda_{cyc} = 1$, and $\lambda_{idt} = 1$. For the text prompt, c_X for generator G_X is ‘‘frozen section,’’ and c_Y for generator G_Y is ‘‘paraffin section.’’

C. Metrics

We employ Frechet Inception Distance (FID) [27] and Kernel Inception Distance (KID) [28] scores to measure whether the generated images match the FFPE data distribution, following the implementation of clean-FID. Smaller values of FID and KID indicate better translation performance of the model. For evaluation, we select the best model based on the validation set. We then translate 10,000 FF images in test dataset into FFPE images and calculate the FID and KID scores between the generated FFPE images and the real FFPE images in the test dataset.

D. Comparison Experiments

We compare our methods with GAN-based methods including CycleGAN [6], CUT [7] and AI-FFPE [8], and diffusion-based methods EGSDE [21] and UNSB [29].

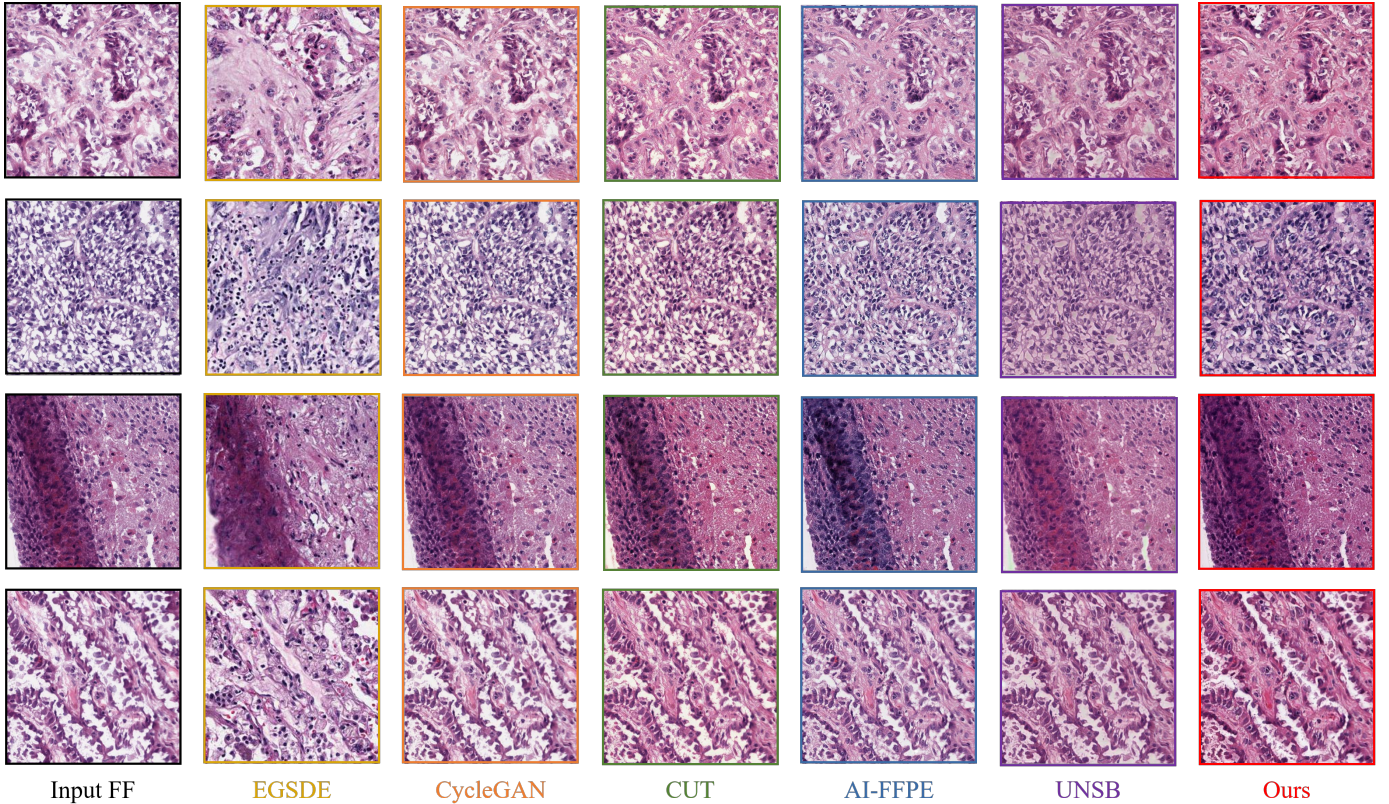


Fig. 2. Visualization results of different methods. The images from left to right are the input FF images, and the FFPE images generated by EGSDE, CycleGAN, CUT, AI-FFPE, UNSB and our proposed Diffusion-FFPE, respectively.

TABLE I
THE PERFORMANCE OF DIFFERENT METHODS
ON TCGA-LUSC AND TCGA-LUAD DATASETS

Model	CycleGAN [6]	CUT [7]	AI-FFPE [8]	EGSDE [21]	UNSB [29]	Diffusion-FFPE (Ours)
FID	34.85	33.86	25.90	62.69	36.37	15.78
KID ($\times 10^3$)	26.00	22.39	17.42	61.28	26.94	8.17

For GAN-based methods, we follow the implementation described in AI-FFPE. For EGSDE, we first train a diffusion model for 1,400,000 steps in the FFPE domain, following the approach outlined in [30], achieving the FID score of 43.11. We then implement EGSDE based on this FFPE-domain diffusion model. Considering the computational overhead, we trained both the diffusion model and EGSDE on images with a resolution of 256x256 pixels. We trained UNSB for 2,000,000 steps according to its specified settings.

E. Results

The performance of different methods on TCGA-LUSC and TCGA-LUAD dataset is shown in Fig. 2 and Table I. Our methods achieve the FID score of 15.78 and the KID score of 8.17×10^{-3} , outperforming other methods. Fig. 2 demonstrates that our method effectively corrects stromal freezing artifacts that introduce blank spaces into the tissue. Fig.3 shows that

our method can achieve a favorable result within a relatively short number of training steps.

As shown in Fig. 2, EGSDE [21] uses downsampled thumbnails to guide diffusion model generation, which makes it difficult to retain the original image’s content and leads to significant discrepancies between the generated FFPE images and the original ones. Additionally, it requires more computation to train a diffusion model that closely matches the FFPE image domain. To preserve image content, both AI-FFPE [8] and UNSB [21] use patch-wise noise contrastive estimation (NCE) loss for regularization, similar to CUT [7]. Specifically, AI-FFPE introduces self-regularization using the L1 norm to align the original image with the generated image. Compared to these methods, the FFPE images produced by our approach have a more pronounced FFPE style, allowing for a clear distinction between tissue and blank areas, while correcting for as many artifacts within the tissue as possible.

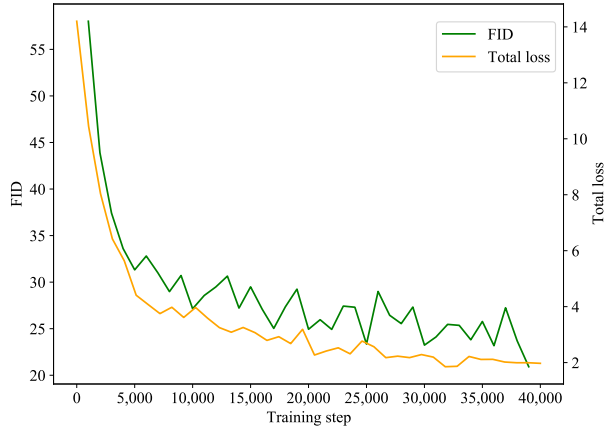


Fig. 3. The curves of FID and total loss over the training steps of Diffusion-FFPE. The FID is obtained from the validation set evaluation. The FID and total loss decrease significantly within the first 5000 training steps.

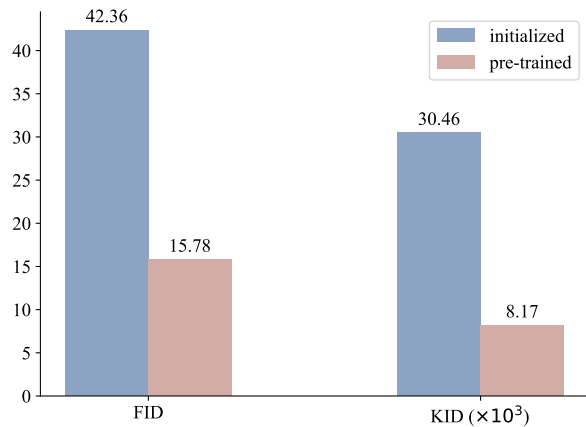


Fig. 4. Comparative analysis of performance with and without pre-trained weights in generator. After utilizing pre-trained model weights, both FID and KID showed significant reductions, with FID decreasing by 26.58 and KID decreasing by 22.29×10^{-3} .

V. ABLATION STUDY

To further explore the impact of using pre-trained models in the generator and discriminator, as well as the effect of the multi-scale feature fusion module, we conduct ablation studies in this section. The model selection and evaluation are the same as described in Section IV-C.

A. The Impact of Utilizing Pre-trained Weights in Generator

To verify that the prior knowledge of the generative model contributes to the generation of FFPE images, we train the model with randomly initialized pre-trained weights in VAE and UNet models of the generator.

As shown in Fig 4, the model with pre-trained weights performs significantly better than the model with randomly initialized weights in terms of FID and KID scores. This

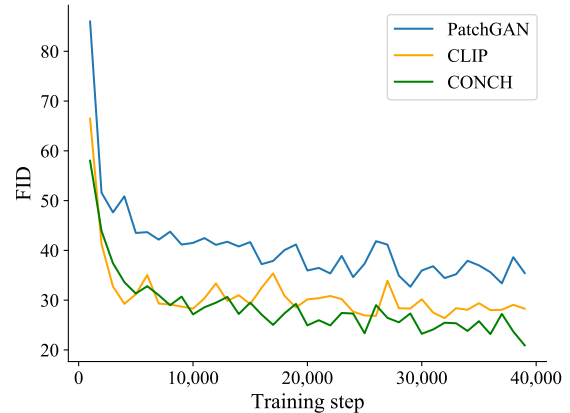


Fig. 5. The curves of the FID over the training steps of the method with PatchGAN, CLIP and CONCH as the backbone of the discriminator. The FID is obtained from the validation set evaluation. Compared to PatchGAN and CLIP, CONCH as the backbone of the discriminator achieves a lower FID score.

TABLE II
COMPARATIVE ANALYSIS OF PERFORMANCE WITH DIFFERENT DISCRIMINATORS

Backbone	Pre-trained Weights	FID	KID ($\times 10^3$)
PatchGAN	×	26.85	17.54
CLIP	✓	19.47	10.37
CONCH	✓	15.78	8.17

demonstrates that the pre-trained weights are crucial for achieving high quality generated results.

B. The Impact of Utilizing Pre-trained Weights in Discriminator

To analyze the impact of employing histopathology pre-trained models as the backbone of the discriminator, we compared experimental results using randomly initialized PatchGAN [31], Contrastive Language-Image Pre-training (CLIP) model [32], and CONCH [15] as discriminator.

As shown in Table II and Fig 5, the discriminator with CONCH as the backbone outperforms the others based on FID and KID metrics. Fig. 6 shows that the FFPE images generated using different discriminators all have satisfactory quality, with only subtle differences. However, using CLIP as the backbone for the discriminator can cause certain color-highlighted areas to appear red. The results suggest that CONCH, as a language-visual model specifically pre-trained for pathology, can improve the performance of the model.

C. The Impact of Multi-scale Feature Fusion Module

Our proposed multi-scale feature fusion (MFF) module integrates features from each layer of both the global VAE encoder and the local VAE encoder. To investigate the influence of the MFF module on the generation performance, we conducted

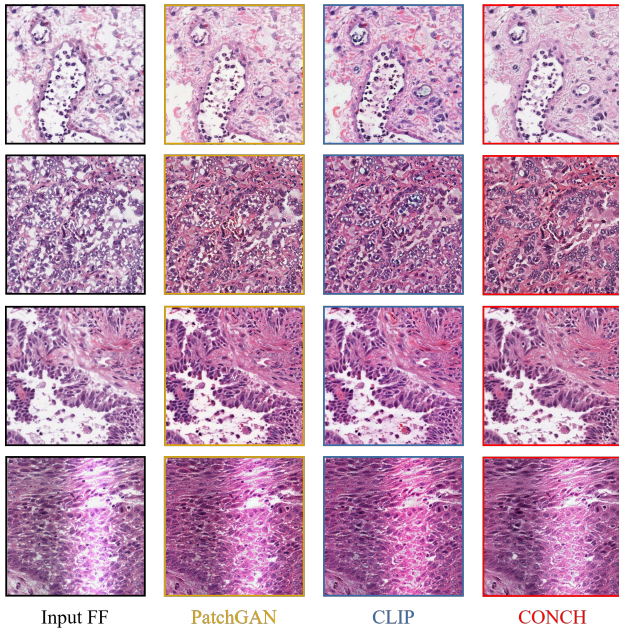


Fig. 6. Visualization results of diffusion FFPE with different discriminators. The images from left to right are the input FF images and the FFPE images generated by PatchGAN, CLIP and CONCH as the backbone of the discriminator, respectively.

TABLE III
COMPARATIVE ANALYSIS OF PERFORMANCE WITH AND WITHOUT
MULTI-SCALE FEATURE FUSION

Multi-scale Feature Fusion	FID	KID ($\times 10^3$)
Not used	18.15	9.75
Last layer	16.24	8.97
Each layer	15.78	8.17

three sets of experiments: one without using the MFF module, one with fusion only on the features of the last layer, and one with fusion on all layers of the VAE encoder.

As shown in Table III, MMF slightly improves the model’s performance on the quantitative metrics FID and KID. Fig. 7 shows that experiments without MMF produce numerous red spots, which is undesirable. Experiments with MMF either on the last layer or on each layer effectively mitigate this problem in the generated results. This improvement is due to the ability of the local VAE encoder to focus on more localized features, thereby preventing the inadvertent introduction of red blood cells into the images.

VI. CONCLUSION

In this paper, we propose Diffusion-FFPE, a method that utilizes pre-trained models for FF-to-FFPE histopathological image translation. Our approach employs a pre-trained one-step diffusion model as the generator, leveraging its generative prior knowledge effectively. Additionally, a pre-trained vision

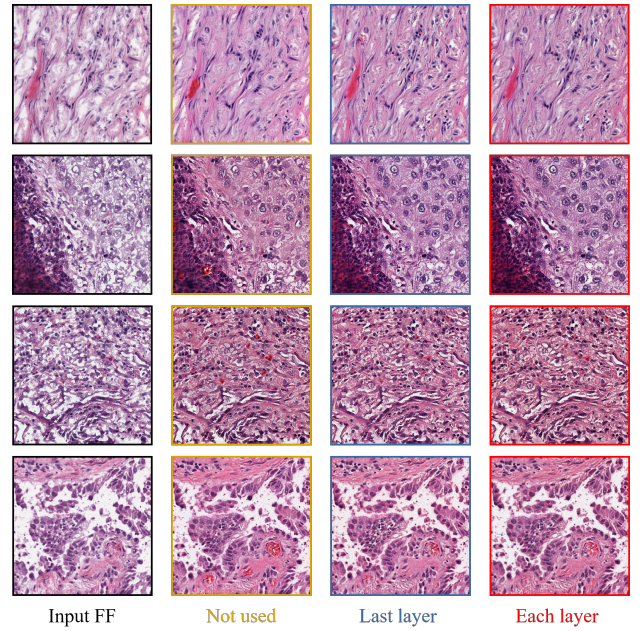


Fig. 7. Visualization results of Diffusion-FFPE with varying settings in the multi-scale feature fusion (MMF) module. The images from left to right show the input FF images and the FFPE images generated without using MMF, with MMF in the last layer, and with MMF in each layer, respectively.

model for histopathology serves as the discriminator backbone to support the GAN training. We also introduce a multi-scale feature fusion module that improves detail translation by focusing on smaller image regions. Our model achieves the FID score of 15.78, outperforming other methods. Moreover, this approach can be extended to FF-to-FFPE image translation tasks in various organs and tissues.

REFERENCES

- [1] C. Rogers, E. Klatt, and P. Chandrasoma, “Accuracy of frozen-section diagnosis in a teaching hospital.” *Archives of pathology & laboratory medicine*, vol. 111, no. 6, pp. 514–517, 1987.
- [2] H. Jaafar, “Intra-operative frozen section consultation: concepts, applications and limitations,” *The Malaysian journal of medical sciences: MJMS*, vol. 13, no. 1, p. 4, 2006.
- [3] H. E. Trejo Bittar, P. Incharoen, A. D. Althouse, and S. Dacic, “Accuracy of the iaslc/ats/ers histological subtyping of stage i lung adenocarcinoma on intraoperative frozen sections,” *Modern Pathology*, vol. 28, no. 8, pp. 1058–1063, 2015.
- [4] K. Falahkheirhah, T. Guo, M. Hwang, P. Tamboli, C. G. Wood, J. A. Karam, K. Sircar, and R. Bhargava, “A generative adversarial approach to facilitate archival-quality histopathologic diagnoses from frozen tissue sections,” *Laboratory Investigation*, vol. 102, no. 5, pp. 554–559, 2022.
- [5] I. Goodfellow, J. Pouget-Abadie, M. Mirza, B. Xu, D. Warde-Farley, S. Ozair, A. Courville, and Y. Bengio, “Generative adversarial nets,” *Advances in neural information processing systems*, vol. 27, 2014.
- [6] J.-Y. Zhu, T. Park, P. Isola, and A. A. Efros, “Unpaired image-to-image translation using cycle-consistent adversarial networks,” in *Proceedings of the IEEE international conference on computer vision*, 2017, pp. 2223–2232.
- [7] T. Park, A. A. Efros, R. Zhang, and J.-Y. Zhu, “Contrastive learning for unpaired image-to-image translation,” in *Computer Vision–ECCV 2020: 16th European Conference, Glasgow, UK, August 23–28, 2020, Proceedings, Part IX 16*. Springer, 2020, pp. 319–345.

- [8] K. B. Ozyoruk, S. Can, B. Darbaz, K. Bařak, D. Demir, G. I. Gokceler, G. Serin, U. P. Hacisalihoglu, E. Kurtuluř, M. Y. Lu *et al.*, “A deep-learning model for transforming the style of tissue images from cryosectioned to formalin-fixed and paraffin-embedded,” *Nature Biomedical Engineering*, vol. 6, no. 12, pp. 1407–1419, 2022.
- [9] L. Fan, A. Sowmya, E. Meijering, and Y. Song, “Fast ff-to-ffpe whole slide image translation via laplacian pyramid and contrastive learning,” in *International Conference on Medical Image Computing and Computer-Assisted Intervention*. Springer, 2022, pp. 409–419.
- [10] Z. Li, Y. Lin, Y. Wang, Z. Fang, H. Bian, R. Hu, X. Li, and Y. Zhang, “St-mksc: The ff-ffpe stain transfer based on multiple key structure constraint,” in *2023 IEEE 20th International Symposium on Biomedical Imaging (ISBI)*. IEEE, 2023, pp. 1–5.
- [11] A. Ramesh, M. Pavlov, G. Goh, S. Gray, C. Voss, A. Radford, M. Chen, and I. Sutskever, “Zero-shot text-to-image generation,” in *International conference on machine learning*. Pmlr, 2021, pp. 8821–8831.
- [12] R. Rombach, A. Blattmann, D. Lorenz, P. Esser, and B. Ommer, “High-resolution image synthesis with latent diffusion models,” in *Proceedings of the IEEE/CVF conference on computer vision and pattern recognition*, 2022, pp. 10 684–10 695.
- [13] D. Podell, Z. English, K. Lacey, A. Blattmann, T. Dockhorn, J. Müller, J. Penna, and R. Rombach, “Sdxl: Improving latent diffusion models for high-resolution image synthesis,” *arXiv preprint arXiv:2307.01952*, 2023.
- [14] K. Zhang and D. Liu, “Customized segment anything model for medical image segmentation,” *arXiv preprint arXiv:2304.13785*, 2023.
- [15] M. Y. Lu, B. Chen, D. F. Williamson, R. J. Chen, I. Liang, T. Ding, G. Jaume, I. Odintsov, L. P. Le, G. Gerber *et al.*, “A visual-language foundation model for computational pathology,” *Nature Medicine*, vol. 30, no. 3, pp. 863–874, 2024.
- [16] R. J. Chen, T. Ding, M. Y. Lu, D. F. Williamson, G. Jaume, A. H. Song, B. Chen, A. Zhang, D. Shao, M. Shaban *et al.*, “Towards a general-purpose foundation model for computational pathology,” *Nature Medicine*, vol. 30, no. 3, pp. 850–862, 2024.
- [17] H. Xu, N. Usuyama, J. Bagga, S. Zhang, R. Rao, T. Naumann, C. Wong, Z. Gero, J. González, Y. Gu *et al.*, “A whole-slide foundation model for digital pathology from real-world data,” *Nature*, pp. 1–8, 2024.
- [18] N. Kumari, R. Zhang, E. Shechtman, and J.-Y. Zhu, “Ensembling off-the-shelf models for gan training,” in *Proceedings of the IEEE/CVF conference on computer vision and pattern recognition*, 2022, pp. 10 651–10 662.
- [19] G. Parmar, T. Park, S. Narasimhan, and J.-Y. Zhu, “One-step image translation with text-to-image models,” *arXiv preprint arXiv:2403.12036*, 2024.
- [20] E. J. Hu, Y. Shen, P. Wallis, Z. Allen-Zhu, Y. Li, S. Wang, L. Wang, and W. Chen, “Lora: Low-rank adaptation of large language models,” *arXiv preprint arXiv:2106.09685*, 2021.
- [21] M. Zhao, F. Bao, C. Li, and J. Zhu, “Egsde: Unpaired image-to-image translation via energy-guided stochastic differential equations,” *Advances in Neural Information Processing Systems*, vol. 35, pp. 3609–3623, 2022.
- [22] X. Su, J. Song, C. Meng, and S. Ermon, “Dual diffusion implicit bridges for image-to-image translation,” *arXiv preprint arXiv:2203.08382*, 2022.
- [23] C. H. Wu and F. De la Torre, “A latent space of stochastic diffusion models for zero-shot image editing and guidance,” in *Proceedings of the IEEE/CVF International Conference on Computer Vision*, 2023, pp. 7378–7387.
- [24] J. Johnson, A. Alahi, and L. Fei-Fei, “Perceptual losses for real-time style transfer and super-resolution,” in *Computer Vision—ECCV 2016: 14th European Conference, Amsterdam, The Netherlands, October 11–14, 2016, Proceedings, Part II 14*. Springer, 2016, pp. 694–711.
- [25] A. Sauer, D. Lorenz, A. Blattmann, and R. Rombach, “Adversarial diffusion distillation,” *arXiv preprint arXiv:2311.17042*, 2023.
- [26] D. P. Kingma and J. Ba, “Adam: A method for stochastic optimization,” *arXiv preprint arXiv:1412.6980*, 2014.
- [27] M. Heusel, H. Ramsauer, T. Unterthiner, B. Nessler, and S. Hochreiter, “Gans trained by a two time-scale update rule converge to a local nash equilibrium,” *Advances in neural information processing systems*, vol. 30, 2017.
- [28] M. Bińkowski, D. J. Sutherland, M. Arbel, and A. Gretton, “Demystifying mmd gans,” *arXiv preprint arXiv:1801.01401*, 2018.
- [29] B. Kim, G. Kwon, K. Kim, and J. C. Ye, “Unpaired image-to-image translation via neural schrödinger bridge,” *arXiv preprint arXiv:2305.15086*, 2023.
- [30] J. Choi, J. Lee, C. Shin, S. Kim, H. Kim, and S. Yoon, “Perception prioritized training of diffusion models,” in *Proceedings of the IEEE/CVF Conference on Computer Vision and Pattern Recognition*, 2022, pp. 11 472–11 481.
- [31] P. Isola, J.-Y. Zhu, T. Zhou, and A. A. Efros, “Image-to-image translation with conditional adversarial networks,” in *Proceedings of the IEEE conference on computer vision and pattern recognition*, 2017, pp. 1125–1134.
- [32] A. Radford, J. W. Kim, C. Hallacy, A. Ramesh, G. Goh, S. Agarwal, G. Sastry, A. Askell, P. Mishkin, J. Clark *et al.*, “Learning transferable visual models from natural language supervision,” in *International conference on machine learning*. PMLR, 2021, pp. 8748–8763.